Soft Matter

Accepted Manuscript

ROYAL SOCIETY OF CHEMISTRY

www.rsc.org/softmatter

Molecular modeling of membrane responses to the adsorption of rotating nanoparticles: promoted cell uptake and mechanical membrane rupture

Tongtao Yue,[a] Xianren Zhang[b] and Fang Huang[*a]

[a]*State Key Laboratory of Heavy Oil Processing, Center for Bioengineering and Biotechnology, China University of Petroleum (East China), Qingdao, 266580, China. E-mail: fhuang@upc.edu.cn*

[b]*Division of Molecular and Materials Simulation, State Key Laboratory of Organic-Inorganic Composites, Beijing University of Chemical Technology, Beijing 100029, China*

Abstract

Recently, a unique dynamic magnetic field was developed to induce rotational movement of superparamagnetic iron oxide nanoparticles. This technique has been applied to remotely control both cellular internalization and apoptosis. Therefore, a thorough understanding of how lipid membrane responds to the introduction of rotating NPs is quite important to promote the applications of this technique in a variety of biomedical area. Here, we performed dissipative particle dynamics (DPD) simulations to systematically investigate the interaction mechanism between lipid membrane and rotating NPs. Two kinds of membrane responses are observed. One is the promoted cell uptake and the other is the mechanical membrane rupture. The promoting effect of NP rotation on cell uptake is ascribed to the enhanced membrane monolayer protrusion, which can wrap the NP from the top side. Meanwhile, the rotating NP exerts a shearing force on the membrane. Accordingly, the membrane undergoes a local distortion around the NP. If the shearing force exceeds a critical value, the local membrane distortion develops into a mechanical rupture. A number of factors, like NP size, NP shape, ligand density and rotation speed, are critical in both above membrane responses.

1. Introduction

In recent years, nanotechnology has opened new avenues in the field of biomedicine.[1,2] In particular, nanoparticles (NPs) with different physicochemical properties have been designed for clinical diagnostics and therapeutics.[3,4] In order to play bio-functions, NPs generally need to transport across the membrane and internalize into the target cell. However, accumulating evidence suggests that NPs may cause adverse health effects during and after their cellular internalization.[5,6] Therefore, understanding how NPs interact with lipid membrane can provide useful guidelines for the safe applications in biomedicine.

In general, the particular internalization pathways for NPs, like receptor mediated endocytosis and membrane penetration, are quite dependent on their own properties, like NP size, shape anisotropy, hydrophobicity, surface charge, and ligand arrangement. For example, the optimal NP size for endocytosis is on the order of 25-50 nm, while exceedingly large or small NPs would yield inefficient uptake.[7-10] Recently, a number of simulation works suggested that the membrane translocation of anisotropic NPs is often accompanied by spontaneous rotation of NPs. For example, by simulating the membrane translocation of ellipsoidal NPs, Yang and Ma observed the NP rotation a consequence of the membrane resistance.[11] The similar behavior was subsequently found for the translocation of ligand coated NPs with anisotropic pattern.[12] Recently, simulation studies demonstrated the spontaneous rotation of graphene sheets during their translocation across membrane.[13] In the endocytosis process of anisotropic NPs, the situation is different. In fact, once approached by NPs, the membrane generally undergoes a local deformation to wrap the NPs and thus leads to cell uptake. Energetically, the NP wrapping is a competition of membrane bending energy and NP-membrane adhesion energy. In order to minimize the free energy, the anisotropic NPs generally undergo a transient rotation during the wrapping process.[14-17] Spontaneous rotation of multiple shaped NPs was also observed as a result of the membrane mediated interactions between adjacent NPs.[18] In general, the spontaneous rotation of anisotropic NPs is transient and has limited effect on the NP-membrane interaction. The active and continuous NP rotation, by contrast, affects

the NP-membrane interaction in a different manner. To our knowledge, however, the active and continuous NP rotation and its effect on the NP-membrane interaction were not considered in previous simulation works.

Compared with the passive and transient NP rotation, the question of how membrane responds to the active rotational NPs is not well understood. In reality, the typical example is the magnetic iron oxide NPs under magnetic field. More recently, Zhang *et al.* developed a dynamic magnetic field approach that can precisely control the rotation of magnetic NPs around their own axis.[19] This enables to induce apoptosis *via* mechanical forces exerted on membranes by targeted NPs. Nevertheless, the interaction of NPs with membrane is very complex. It depends on both NP properties, like NP size,[7-10] NP shape,[11-18, 20, 21] NP elasticity,[22,23] NP concentration[24-26] and ligand properties,[12 ,27-29] and membrane properties, like membrane tension,[30] membrane asymmetry,[31] and transmembrane potential.[32] Besides, when the active NP rotation is turned on, the NP-membrane interaction will be rather different. Typically, different membrane responses will be strongly affected by the shearing force generated by the oscillatory torques of rotating NPs.

In this work, we performed Dissipative Particle Dynamics (DPD) simulations to systematically investigate the interaction mechanism between membrane and rotating NPs. Depending on the NP size, NP shape, ligand density and NP rotating speed, two kinds of membrane responses are observed: promoted cell uptake and mechanical membrane rupture. The former membrane response provides an effective pathway for the enhanced cellular internalization of NPs, while the later membrane response is related to cytotoxicity. These results support the recent experimental reports that both cellular internalization and apoptosis can be remotely controlled by regulating external magnetic field.[19]

2. Model and Simulation Methods

2.1 Model

The coarse-grained models of different components in our simulations are shown in Figure 1. A model lipid molecule is constructed by connecting one hydrophilic bead

(H) to three hydrophobic beads (T). The H1T3 lipid model can self assemble into the planar and vesicular membranes. In order to save computer time, we prepare the planar membrane by initially arranging a number of lipids in a defined plane. Before addition of NPs, the initial system was equilibrated for about 100000 DPD time steps. The coarse-grained lipid model (H1T3) was first used to investigate the dynamics of domain growth in multi-component lipid vesicles.[33] Recently, we applied this model to simulate the morphology transformation mechanism of membrane tubes.[34] In order to model the specific receptor-ligand interaction, 50% of lipids in the membrane are set to behave as receptors (R), which interact with ligands on the NP surface (Fig. 1A). Each NP is constructed by arranging the hydrophilic beads (P) and is constrained to move as a rigid body (Fig. 1D-F). Water molecules, which are modeled as single beads (W), and other components are not allowed to enter the interior of NPs. To explore the effect of NP size, spherical NPs with different diameters, including D = 10 nm, 12.5 nm, 15 nm, 17.5 nm and 20 nm, are constructed. For the effect of NP shape, we construct cylindrical NPs with the same volume (1900 nm^3) but different aspect ratios, including L/D = 20:11, 13.5:13.5 and 8.0:17.4. The ligands coating on the NP surface were modeled as single solid beads (L) and are set to interact with the hydrophilic bead of each receptor.

2.2 DPD simulation method

The simulations presented in this work are based on the Dissipative Particle Dynamics (DPD) method, which is a coarse-grained simulation technique with hydrodynamic interaction. The DPD method was first introduced to simulate the hydrodynamic behavior of complex fluids[35-37] and proved to be especially useful in studying the mesoscale behaviors of lipid membranes.[38-41] In DPD, the dynamics of the elementary units is governed by Newton's equation of motion $dr_i/dt = v_i$ and $dv_i/dt = f_i/m$, similar to the molecular dynamics method. Typically, in the DPD, there are three different pairwise forces acting on bead i by bead j: the conservative force F_{ij}^C, dissipative force F_{ij}^D, and random force F_{ij}^R. So the total force exerted on bead i by bead j can be

expressed as

$$F_i = \sum_{i \neq j} (F_{ij}^C + F_{ij}^D + F_{ij}^R) \quad (1)$$

The conservative force between beads i and j is used to model the repulsive interactions of beads i and j and is determined by

$$F_{ij}^C = a_{ij} \tilde{r}_{ij} \max\{1 - r_{ij}/r_c, 0\} \quad (2)$$

where a_{ij} is the maximum repulsive strength between beads i and j, $\boldsymbol{r_{ij}}=\boldsymbol{r_j}-\boldsymbol{r_i}$ ($\boldsymbol{r_i}$ and $\boldsymbol{r_j}$ are their positions), $r_{ij} = |\boldsymbol{r_{ij}}|$, $\tilde{r}_{ij} = \boldsymbol{r_{ij}}/r_{ij}$, and r_c is the cut off radius. The interaction parameter is determined according to the hydrophobicity of two interacting beads. Specifically, we take the repulsive parameter $a_{ii} = 25$ for any two beads of the same type. For two beads of different types, we set the interaction parameter to denote the hydrophilic/hydrophobic property of the beads as follows: $a_{ij} = 25$ if the two beads are both hydrophilic or both hydrophobic, while $a_{ij} = 200$ if one is hydrophobic and the other is hydrophilic. In order to model the receptor-ligand interaction, we set the parameter $a_{R_H L} = 0$.

The dissipative force has the form,

$$F_{ij}^D = -\gamma(1 - r_{ij}/r_c)^2 (\tilde{r}_{ij} \cdot v_{ij}) \tilde{r}_{ij} \quad (3)$$

where γ is the friction coefficient, $v_{ij} = v_i - v_j$ (v_i and v_j are their velocities). The expression is chosen to conserve the momentum of each pair of particles and thus the total momentum of the system is conserved.

The random force also acts between each pair of particles as

$$F_{ij}^R = -\sigma(1 - r_{ij}/r_c)^2 \theta_{ij} \tilde{r}_{ij} \quad (4)$$

where σ represents the noise amplitude, and θ_{ij} is an uncorrelated random variable with zero mean and unit variance.

Within a lipid molecule, a harmonic spring force is applied to connect two neighboring beads,

$$F_S = K_S (r_{ij} - r_{eq}) \tilde{r}_{ij} \quad (5)$$

where K_S and r_{eq} are the spring constant and equilibrium bond length, respectively.

The numerical values of K_S and r_{eq} used for our simulations are 128 and 0.7, respectively.

In order to ensure the rigidity of lipids, the force constraining the variation of bond angle is given by

$$F_\varphi = -\nabla U_\varphi \quad \text{and} \quad U_\varphi = K_\varphi(1-\cos(\varphi-\varphi_0)) \tag{6}$$

where φ_0 is set to π and K_φ, the bond bending force constant, is set to 10.0.

In DPD simulations, we apply the velocity-verlet integration algorithm and the integration time step $\Delta t = 0.02\tau$. The cutoff radius r_c, bead mass m, energy k_BT are chosen as the simulation units. The periodic boundary conditions are adopted in all three directions. The initial size of the simulation box is $60r_c \times 60r_c \times 60r_c$ with the number density of 3. The reduced DPD units can be converted to SI units by mapping the membrane thickness and lipid diffusion coefficient. In experiments, the thickness of a lipid bilayer is of the order of 5 nm and the in-plane diffusion constant of lipids is about 5.0 $\mu m^2 s^{-1}$. Accordingly, one DPD length unit corresponds to approximately 1.25 nm in physical units and the time unit to τ = 30 ps. All simulations are performed in the N-varied VT ensembles, in which the targeted membrane tension can be controlled by monitoring the number of lipids per area in a boundary region. The detailed description of N-varied DPD simulation method is given in the following section.

In order to model the active NP rotation, we switch off the spontaneous NP rotation when the wrapping percentage achieves a specific value. Meanwhile, the active NP rotation is switched on by redefining the rotation matrix according to different rotation speed. In reality, the speed of NP rotation can be controlled by varying the frequency setting on the dynamic magnetic field device.[19] For example, the frequency was set to be 10~20 Hz in recent experiments.[19] Previously, the high frequent NP rotation (kHz-MHz) was also applied to induce the NP rotation.[42,43] In this work, the NP rotation speed is in the range of 0.2~1.0 degree/ns. Accordingly, the NPs are expected to rotate about 3.33~16.67 cycles during the simulation time of 6.0μs. It should be noted that the NP rotation speed is much larger than those used in the

experiments. This is mainly because of the extremely high computational cost to simulate the membrane rupture under low NP rotation speed.

2.3 N-varied DPD simulation method

In this work, the N-varied DPD simulation method, a particular variant of the DPD method,[44] was applied to simulate the interaction between rotating NPs and membrane. In the N-varied DPD method, the targeted membrane tension can be controlled by monitoring the number of lipids per area (LNPA) in the membrane boundary region. The boundary region, which surrounds the central square region of the membrane, thus plays a role as a reservoir of lipids. By addition/deletion moves of lipids, the value of LNPA in the boundary region is kept within a defined range ($\rho_{LNPA}^{\min} < \rho_{LNPA} < \rho_{LNPA}^{\max}$). In an addition move, a number of lipid molecules are inserted into the boundary region if the local lipid area density is less than $\rho_{LNPA}^{\min}$. Conversely, if the average area density of lipids in the boundary region exceeds $\rho_{LNPA}^{\max}$, a corresponding number of lipids are deleted randomly from the boundary region. Simultaneously, a corresponding number of water beads is randomly added or deleted to keep the whole density of beads in the simulation box constant. In practice, the value of ρ_{LNPA} is fixed to 1.45 to make the membrane tension fluctuate around zero. The addition or deletion move is performed every 1500 time steps in order to leave enough time to propagate the membrane tension to the whole membrane.

3. Simulation Results and Discussion

In this work, we concentrate on the membrane responses to the adsorption of rotating NPs. On one hand, the cell uptake can be promoted by active NP rotation. On the other hand, the rotating NPs exert a shearing force on the membrane and thus may induce the mechanical membrane rupture. In reality, both membrane responses can be utilized for different applications in the field of nanomedicine. Recently, the dynamic magnetic field approach was applied to induce rotation of individual magnetic NPs.

Once internalized into the targeted cell, the rotational NP movement can be used for remote induction of cell death by injuring the lysosomal membrane structures.[19] Besides the controlled cell death induced by NP rotation, the efficiency of cellular uptake of rotating NPs is equally important, especially when NPs are used to deliver drug into the targeted cells. This is speculated because the rotating NPs exert a shearing force on cellular membrane that would change the mechanical property and even the fluidity of the membrane. As a result, the efficiency of cell uptake is expected to be affected by the active NP rotation. To optimize the conditions for applications of this technology, a systematic understanding of interaction between membrane and rotating NPs is thus in urgent need.

3.1 Cell uptake promoted by NP rotation

First, the NP diameter and ligand number are set to D = 15 nm and N_L = 261, respectively. The NP rotation with speed of V = 0.2 degree/ns and V = 0.47 degree/ns are switched on when the wrapping percentage achieves 60%. To highlight the effect of active NP rotation on cell uptake, we performed one control simulation without active NP rotation. For free NP, the wrapping completes in about 2.25μs (Fig. 2A). Besides, the NP wrapping is in some extent mediated by the membrane monolayer protrusion, which has been observed in our previous simulation work.[32] When the active NP rotation with a speed of V = 0.2 degree/ns is turned on, the wrapping is obviously promoted and completes in about 0.99μs (Fig. 2B, D). Furthermore, as the rotation speed is increased to V = 0.47 degree/ns, the NP wrapping is further promoted and completes in about 0.6μs (Fig. 2C, D).

On a molecular level, as the NP rotation proceeds, a number of lipid molecules adjacent to the NP is stretched out of the membrane and adsorb on the NP surface (Fig. 1B, 0.45μs). As a result, the membrane monolayer protrusion keeps growing along the NP surface and wraps the NP from the top side (Video S1). After the wrapping completes, the NP continues rotating and thus exerts a shearing force on the membrane. Accordingly, the membrane undergoes a severe distortion around the NP. In order to further illustrate the promoting effect of NP rotation on the cell uptake, we

compared the wrapping completion time under different NP rotation speed. The enhancement is confirmed by continuous decrease of wrapping completion time as a function of NP rotation speed (Fig. 2E). Nevertheless, as the NP rotation speed exceeds $V = 0.2$ degree/ns, the wrapping completion time keeps decreasing but with a smaller gradient. We speculate that the NP undergoes a slipping on the membrane, which in some extent reduces the promoting efficiency.

Next, we compared the wrapping of rotating NPs with different size. The NP rotation with speed of $V = 0.47$ degree/ns is turned on when the wrapping percentage achieves 30%. We chose five different NP diameters, including $D = 10$ nm, $D = 12.5$ nm, $D = 15$ nm, $D = 17.5$ nm, and $D = 20$ nm. It is noteworthy that the wrapping is more efficient for larger NPs in the absence of active NP rotation. This is because the membrane bending energy is effectively reduced by increasing NP size. However, when the active NP rotation is turned on, the cell uptake is always enhanced and the wrapping dynamics is changed. In this case, the role of membrane monolayer protrusion is amplified, while the membrane bending energy is less critical. Therefore, under the same rotation speed, it will take longer time to wrap a larger NP. Indeed, the time evolution of wrapping percentage for rotating NPs with different size conforms that the cell uptake is more efficient for smaller NPs (Fig. 3).

As the membrane monolayer protrusion, which promotes the cell uptake of NPs, is derived from the receptor-ligand interaction, we next compared the cell uptake of rotating NPs with different ligand density. The rotation speed and NP diameter are fixed to $V = 0.57$ degree/ns and $D = 15$ nm, respectively. In general, the receptor-ligand interaction is enhanced by increasing the ligand density. Accordingly, one step NP rotation will stretch more lipid molecules out of the membrane and thus the membrane monolayer protrusion is promoted. The promoting effect is clearly illustrated in the time evolution of wrapping percentage, which shows that the efficiency of cell uptake is promoted by increase of the ligand density (Fig. 4A). However, as we further increase the ligand density, the wrapping efficiency is contrarily reduced (Fig. 4B). This phenomenon again verifies the existence of NP slipping on the membrane.

Before our simulations, it was thought that the cell uptake efficiency can always be increased by increasing the rotation speed or ligand density. This is because increasing the NP rotation speed can promote the membrane monolayer protrusion, while increasing the ligand density can increase the NP-membrane adhesion strength. However, our simulations suggest that the effect of both rotation speed and ligand density on cell uptake efficiency is staged. First, the wrapping completion time decreases with the increase of both rotation speed (Fig. 2) and ligand density (Fig. 4). However, further increase of rotation speed is found to decrease the gradient, with which the wrapping completion time decreases. Moreover, when the ligand density exceeds a critical value, the wrapping completion time contrarily increases with further increase of the ligand density. Both above phenomenon suggest that the rotational NPs undergo different extent of slipping on the membrane, which in some extent reduces the cell uptake efficiency.

It is noteworthy that the NP slipping is general in our simulations, and is more obvious for higher rotation speed and larger ligand density. In order to confirm the existence of NP slipping, we fixed the NP diameter and rotation speed to D = 15 nm and V = 0.57 degree/ns, respectively. Two ligand densities were compared. They are N_L = 298 and N_L = 890, respectively. The extent of NP slipping is quantified by counting the lipid molecules which were bound to ligands in the former step but free in the current step. As the NP-membrane contact area keeps increasing during the wrapping process, the slipping number increases until the wrapping completes (Fig. 5). On a molecular level, the active NP rotation is accompanied by broken of receptor-ligand bindings. Comparatively, the receptors detached from old ligands can bind new ligands more easily for NPs with higher ligand density. Therefore, the slipping of NPs with higher ligand density is more obvious than that of NPs with lower ligand density (Fig. 5).

3.2 Mechanical Membrane rupture induced by NP rotation

In the above section, we mentioned that the rotating NP exerts a shearing force on the membrane. As a result, the membrane undergoes a severe distortion around the NP

(Fig. 2C, 0.78μs). We speculate that the severe membrane distortion may develop into a mechanical rupture if the shearing force exceeds a critical value. In general, the shearing force is affected by several factors, like NP rotation speed, NP size, shape anisotropy and ligand density. First, we fixed the NP diameter and ligand number to D = 15 nm and N_L = 261, respectively, and increase the rotation speed to V = 0.57 degree/ns. As shown in the typical snapshots, the NP is first wrapped by the membrane (Fig. 6). Meanwhile, the membrane undergoes a severe local distortion as the wrapping completes (Fig. 6, 0.78μs). Subsequently, the distortion develops into a membrane rupture adjacent to the NP. As the simulation proceeds, the membrane rupture develops into a larger membrane pore and the wrapped NP keeps rotating and has a tendency to curl over the membrane (Fig. 6, 3.0μs, Video S2).

The effect of NP size is shown in the typical snapshots (Fig. 7). The rotation speed is fixed to V = 0.57 degree/ns, under which the membrane undergoes a mechanical rupture by rotating a NP with diameter of D = 15 nm (Fig. 6). However, as we decrease the NP diameter to D = 12.5 nm, no membrane rupture is observed during our simulation. Besides, after wrapping completes, the wrapped NP keeps rotating and translating in the membrane (Fig. 7A). Contrarily, as we increase the NP diameter to D = 20 nm, the NP-membrane contact area is increased and thus the shearing force is strengthened. As a result, the membrane undergoes a mechanical rupture before completion of the wrapping (Fig. 7B). Therefore, the membrane response to rotating NPs is strongly affected by the NP size.

Next, we compare the membrane responses to rotating NPs with different shape anisotropy. To this end, we fixed the cylindrical NP volume and varied the aspect ratio, including L:D = 20:11, L:D = 13.5:13.5, and L:D = 8.0:17.4, respectively. The NP rotation speed is set to V = 0.57 degree/ns. After the wrapping completes, the membrane undergoes a mechanical rupture in all three cases (Fig. 8). Nevertheless, we compare the situation with that of spherical NPs. In general, the magnitude of shearing force determines whether or not the membrane undergoes mechanical rupture, while the rupture location and occasion are strongly affected by rotation direction and instantaneous NP orientation. On one hand, the mechanical membrane

rupture always occurs at left side of the NP if the NP rotation is clockwise. On the other hand, when interacting with anisotropic NPs, the occasion of membrane rupture is dependent on the instantaneous orientation of NPs with respect to the membrane. Specifically, the shearing force exerted by rotating NPs is maximized when the longer edge of NP is parallel with the membrane (arrows in Fig. 8).

In the above section, we showed that the rotating NP generally undergoes a slipping, the extent of which is affected by ligand density. Besides, the promoting effect of NP rotation on cell uptake is weakened by the NP slipping. Likewise, the same factor is expected to play a role in the mechanical membrane rupture. Here, we fixed the NP diameter and NP rotation speed to D = 15 nm and V = 0.67 degree/ns, respectively. The ligand number is varied discontinuously from N_L = 114 to as large as N_L = 890. For NPs with lower ligand density (N_L < 200), no membrane rupture is observed during our simulations (Fig. 9A, B). As we increase the ligand density to N_L = 226, the membrane undergoes a rupture after the completion of wrapping (Fig. 9C, 1.35μs). For NPs with ligand density of N_L = 298 (Fig. 9D), the membrane rupture occurs at 3.9μs. The obvious delay of membrane rupture is mainly ascribed to the enhanced NP slipping (Fig. 5). As we further increase the ligand density (Fig. 9E-H), the extent of NP slipping is further enhanced. As a result, the magnitude of shearing force exerted by rotating NPs is contrarily reduced and accordingly no membrane rupture occurs during our simulation. The decreased shearing force is further reflected by the disappearing of membrane distortion around the NP (Fig. 9H).

In general, the lipid membrane undergoes rupture when the surface tension exceeds a critical value. The interaction between water and membrane is thus critical in both thermodynamic and structural stability of the membrane. Theoretically, Wang and Frenkel demonstrated that a stretching lateral pressure would induce the nucleation of pore on the membrane.[45] In this work, we propose that the membrane rupture can also be realized by the active NP rotation. It is explained that the rotational NP can exert a shearing force on the membrane and thus increase the membrane surface tension. Comparatively, the role of water in the membrane damage is much less important and thus will not be discussed. In order to verify the role of NP rotation on the mechanical

property of the membrane, we calculate the time evolution of membrane surface tension for the cases with and without the NP rotation (Fig. 10). The NP diameter and the lipid number pear area are set to D = 15 nm and ρ_{LNPA} = 1.45, respectively. For the case without NP rotation, the surface tension keeps fluctuating around the value of 1.0 k_BT/r_c^2. Accordingly, no membrane rupture was observed at the end of 3μs simulation run. In contrast, when the NP rotation with speed of 0.57 degree/ns is turned on, the membrane tension first undergoes a slight increase, which is induced by the shearing force exerted by the rotational NP. At about t = 1.0μs, an abrupt decline of the membrane tension occurs. Accordingly, the membrane undergoes a rupture to release the surface energy. As the NP keeps rotating and curls over the membrane (Fig. 6), the membrane tension continues to increase after the membrane rupture occurs (Fig. 10). Therefore, it is the NP rotation that provides the driving force for the membrane rupture. As we have known that the NP adsorption can damage the cell membranes and leads to the cell death,[46] here we show that membrane damage can also be realized by the active NP rotation on the membrane surface.

3.3 Phase diagrams

In the above sections, we showed that the rotating NPs can exert shearing force on the membrane. As a result, two membrane responses to the adsorption of rotating NPs are observed. They are the promoted cell uptake and the mechanical membrane rupture. The magnitude of the shearing force, which determines the membrane response, is determined by a number of factors, like NP size, shape anisotropy, ligand density and NP rotation speed. In this section, we performed a large number of simulations and conclude the effect of NP size, ligand density and rotation speed on membrane responses in two phase diagrams.

In the first phase diagram, we fixed the NP diameter to D = 15 nm and conclude the membrane responses in the plane of ligand density and rotation speed (Fig. 11A). When the ligand density is relatively low (for example, N_L = 114), the cell uptake is always promoted by NP rotation. However, the shearing force generated by rotating

NP is too weak to induce the mechanical membrane rupture, even at higher rotation speed. As we increase the ligand density, the NP-membrane adhesion strength and accordingly the shearing force is increased. As a result, the membrane undergoes a rupture by NPs with higher rotation speed. Nevertheless, the increase of ligand density also enhances the NP slipping (Fig. 5), which in turn reduces the shearing force. Indeed, our simulations indicate that the minimum rotation speed for mechanical membrane rupture increases when the ligand density exceeds 300. Furthermore, for NPs with rather high ligand density (for example, N_L = 890), the NP slipping is further enhanced. Accordingly, the shearing force exerted by rotating NP is rather weak and thus no membrane rupture is observed, even at high rotation speed.

Next, we fixed the ligand density and varied the NP diameter and rotation speed. The combined effect on the membrane response is illustrated in the phase diagram (Fig. 11B). For smaller NPs, the promoted cell uptake is more efficient than that of larger NPs (Fig. 3). However, due to the small NP-membrane contact area, the shearing force by rotating NPs is too small to induce the mechanical membrane rupture. Therefore, no membrane rupture is observed unless under rather high rotation speed (D = 10 nm, V = 1.0 degree/ns). As we increase the NP size, the magnitude of shearing force by rotating NPs is effectively enhanced because of larger NP-membrane contact area. Accordingly, the minimum rotation speed required for membrane rupture is effectively decreased. Specifically, for NPs with diameter of D= 20 nm, the membrane is stretched to rupture when the rotation speed is as low as V = 0.2 degree/ns. Besides, when the NP rotation speed is larger than 0.5 degree/ns, the mechanical membrane rupture occurs before the completion of wrapping (Fig.7).

In recent experiments, the dynamic magnetic field was developed to induce the low-frequency NP rotation around its own axis. By this method, both NP uptake into cells and disruption of lysosomal membrane are facilitated.[19] Comparatively, the simulation results presented in this work provide direct insight into the molecular processes underlying the different membrane responses. More importantly, a number of factors, like NP size, NP shape, ligand density and rotation speed, are found to affect the membrane response. Therefore, the present work will promote the potential

applications in the field of biomedicine, like targeted drug delivery. Specifically, we can provide both qualitative and quantitative guidelines to optimize the NP properties to both reduce the side effects and increase the efficiency of cellular internalization.

4. Conclusions

Understanding how NPs having different properties interact with lipid membrane is of quite importance for their safe applications in a variety of biomedicine. Compared with the well understood role of spontaneous NP rotation in both membrane penetration and cell uptake process, the interaction mechanism of membrane with active rotating NPs is less understood. In this work, we performed DPD simulations to suggest that the rotating NPs can exert shearing force on the membrane. Accordingly, two membrane responses are observed. They are the promoted cell uptake and the mechanical membrane rupture. On a molecular level, the promoted cell uptake is mediated by the accelerated membrane monolayer protrusion, which can wrap the NP from the top side. Meanwhile, the membrane undergoes a local distortion as the NP rotation proceeds. If the shearing force exceeds a critical value, the local membrane distortion develops into a mechanical rupture. Our system simulation suggests that the magnitude of shearing force, which determines the membrane response, is affected by a number of factors, like NP rotation speed, NP size, NP shape and ligand density.

In summary, the study reveals two different membrane responses to the adsorption of rotating NPs. The phase diagrams presented here have the potential to provide both qualitative and quantitative guidelines for the application of rotating NPs in a variety of biomedical area. In other words, the study highlights how the properties of NPs and external magnetic field can be modified to yield the required therapeutic efficiency while minimizing the cytotoxicity.

Acknowledgements

This work was financially supported by National Natural Science Foundation of China (No. 21303269, 21273287 and 21033005), the program for New Century Excellent Talents in University of Ministry of Education of China (NCET-10-0815),

and the Natural Science Foundation for Distinguished Young Scholar of Shandong Province (No. JQ201008). T. YUE is grateful for the support of Natural Science foundation of Shandong Province (No. ZR2013BQ029), the Qingdao Science and Technology Project (No. 13-1-4-235-jch), and the Fundamental Research Funds for the Central Universities. The authors thank the National Super-computing Center in Jinan and Shenzhen for providing computer time.

References

1 T. L. Doane and C. Burda, *Chem. Soc. Rev.*, 2012, **41**, 2885-2991.

2 Y. Xia, *Nat. Mater.*, 2008, **7**, 759-760.

3 R. F. Service, *Science*, 2005, **310**, 1132-1134.

4 D. Bechet, P. Couleaud, C. Frochot, M. L. Viriot, F. Guillemin and M. Barberi-Heyob, *Cell*, 2008, **26**, 612-621.

5 P. R. Leroueil, S. Hong, A. Mecke, J. R. Baker JR, B. G. Orr and M. M. B. Holl, *Acc. Chem. Res.*, 2007, **40**, 335-342.

6 C. J. Murphy, A. M. Gole, J. W. Stone, P. N. Sisco, A. M. Alkilany, E. C. Goldsmith and S. C. Baxter, *Acc. Chem. Res.*, 2008, **41**, 1721-1730.

7 W. Jiang, B. Y. S. Kim, J. T. Rutka and W. C. W. Chan, *Nat. Nanotechnol.*, 2008, **3**, 145-150.

8 S. L. Zhang, J. Li, G. Lykotrafitis, G. Bao and S. Suresh, *Adv. Mater.*, 2009, **21**, 419-424.

9 H. Gao, W. D. Shi and L. B. Freund, *Proc. Natl. Acad. Sci. U. S. A.*, 2005, **102**, 9469-9474.

10 R. Lipowsky and H. –G. Döbereiner, *Europhys. Lett.*, 1998, **43**, 219-225.

11 K. Yang and Y. –Q. Ma, *Nat. Nanotechnol.*, 2010, **5**, 579-583.

12 Y. Li, X. Li, Z. Li and H. Gao, *Nanoscale*, 2012, **4**, 3768-3775.

13 Y. Li, H. Yuan, A. von dem Bussche, M. Creighton, R. H. Hurt, A. B. Kane and H. Gao, *Proc. Natl. Acad. Sci. U. S. A.*, 2013, **110**, 12295-12300.

14 X. Yi, X. Shi and H. Gao, *Nano Lett.*, 2014, **14**, 1049-1055.

15 R. Vácha, F. J. Martinez-Veracoechea and D. Frenkel, *Nano Lett.*, 2011, **11**,

5391-5395.

16 C. Huang, Y. Zhang, H. Yuan, H. Gao and S. Zhang, *Nano Lett.*, 2013, **13**, 4546-4550.

17 Y. Li, T. Yue, K. Yang and X. Zhang, *Biomaterials*, 2012, **33**, 4965-4973.

18 T. Yue, X. Wang, F. Huang and X. Zhang, *Nanoscale*, 2013, **5**, 9888-9896.

19 E. Zhang, M. F. Kircher, M. Koch, L. Eliasson, S. N. Goldberg and E. Renström, *ACS Nano*, 2014, **8**, 3192-3201.

20 S. Dasgupta, T. Auth and G. Gompper, *Soft Matter*, 2013, **9**, 5473-5482.

21 S. Dasgupta, T. Auth and G. Gompper, *Nano Lett.,* 2014, **14**, 687-693.

22 X. Yi, X. Shi and H. Gao, *Phys. Rev. Lett.*, 2011, **107**, 098101.

23 T. Yue and X. Zhang, *Soft Matter*, 2013, **9**, 559-569.

24 T. Yue and X. Zhang, *ACS Nano*, 2012, **6**, 3196-3205.

25 K. Jaskiewicz, A. Larsen, D. Schaeffel, K. Koynov, I. Lieberwirth, G. Fytas, K. Landfester and A. Kroeger, *ACS Nano*, 2012, **6**, 7254-7262.

26 B. J. Reynwar, G. Illya, V. A. Harmandaris, M. M. Müller, K. Kremer and M. Deserno, *Nature*, 2007, **447**, 461-464.

27 A. Verma and F. Stellacci, *Small*, 2010, **6**, 12-21.

28 H. –M. Ding and Y. –Q. Ma, *Biomaterials*, 2012, **33**, 5798-5802.

29 H. –M. Ding and Y. –Q. Ma, *Biomaterials*, 2013, **34**, 8401-8407.

30 T. Yue and X. Zhang, *Soft Matter*, 2011, **7**, 9104-9112.

31 T. Yue, X. Zhang and F. Huang, *Soft Matter*, 2014, **10**, 2024-2034.

32 J. Lin and A. Alexander-Katz, *ACS Nano*, 2013, **7**, 10799-10808.

33 M. Laradji and P. B. Sunil Kumar, *Phys. Rev. Lett.*, 2004, **93**, 198105.

34 T. Yue, X. Zhang and F. Huang, *Phys. Chem. Chem. Phys.*, 2014, **16**, 10799-10809.

35 P. J. Hoogerbrugge and J. M. V. A. Koelman, *Europhys. Lett.*, 1992, **19**, 155-160.

36 P. Español and P. Warren, *Europhys. Lett.*, 1995, **30**, 191-196.

37 R. D. Groot and P. B. Warren, *J. Chem. Phys.*, 1997, **107**, 4423-4435.

38 J. C. Shillcock and R. Lipowsky, *Nat. Mater.*, 2005, **4**, 225-228.

39 X. Chen, F. Tian, X. Zhang and W. Wang, *Soft Matter*, 2013, **9**, 7592-7600.

40 N. Arai, K. Yasuoka and X. C. Zeng, *Nanoscale*, 2013, **5**, 9089-9100.

41 M. Dutt, O. Kuksenok, M. J. Nayhouse, S. R. Little and A. C. Balazs, *ACS Nano*, 2011, **5**, 4769-4782.

42 J. H. Lee, J. T. Jang, J. S. Choi, S. H. Moon, S. H. Noh, J. W. Kim, J. G. Kim, I. S. Kim, K. I. Part and J. Cheon, *Nat. Nanotechnol*., 2011, **6**, 418-422.

43 P. Tseng, J. W. Judy and D. Di Carlo, *Nat. Methods*, 2012, **9**, 1113-1119.

44 T. Yue, S. Li, X. Zhang and W. Wang, *Soft Matter*, 2010, **6**, 6109-6118.

45 Z. Wang and D. Frenkel, *J. Chem. Phys.*, 2005, **123**, 154701.

46 N. Lewinski, V. Colvin and R. Drezek, *Small*, 2008, **4**, 26-49.

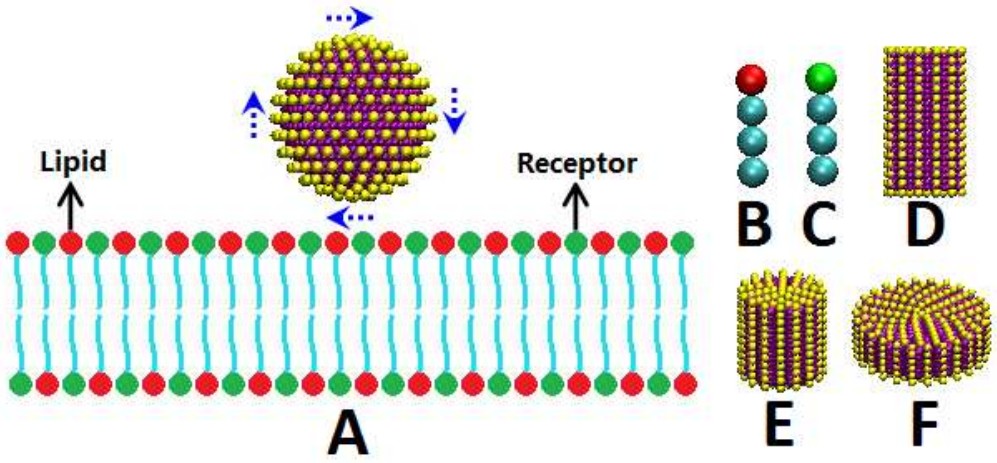

Fig. 1 Schematic representation of interaction between membrane and rotating NP (*D* = 15 nm): (A) different components, (B) lipid molecule, (C) receptor molecule, (D) long rod-like NP (*L/D* = 20:11), (E) short rod-like NP (*L/D* = 13.5:13.5), (F) disk-like NP (*L/D* = 8.0:17.4).

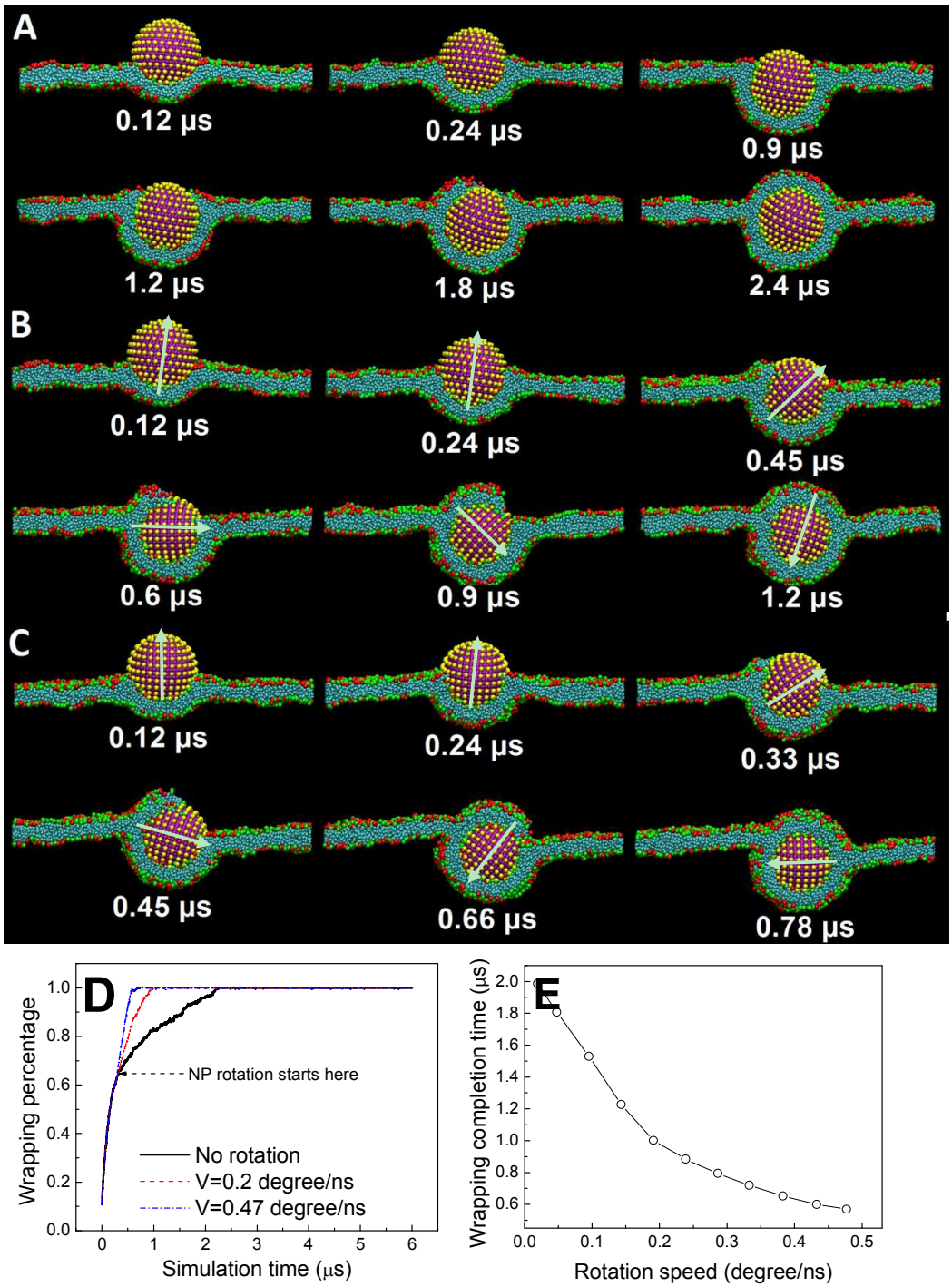

Fig. 2 Promotion of cell uptake by active NP rotation. (A) cell uptake of free NP for comparison, (B) promoted cell uptake of NPs with the rotation speed of V = 0.2 degree/ns, (C) promoted cell uptake of NPs with the rotation speed of V = 0.47 degree/ns, (D) time evolutions of wrapping percentage for free and rotating NPs, (E) wrapping completion time as a function of rotation speed. The arrows show the

instantaneous NP orientation.

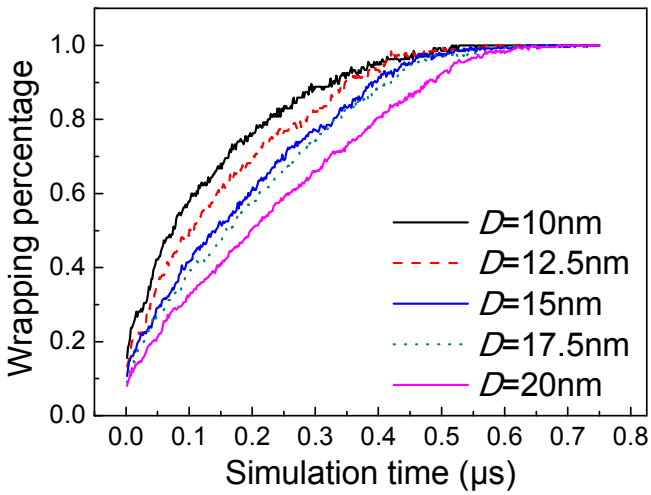

Fig. 3 Effect of NP size on the promoted cell uptake. Five different NP diameters are applied. They are D = 10 nm, 12.5 nm, 15 nm, 17.5 nm, and 20 nm. The NP rotation speed is set to V = 0.47 degree/ns. The arrow shows the trend of decreasing cell uptake efficiency.

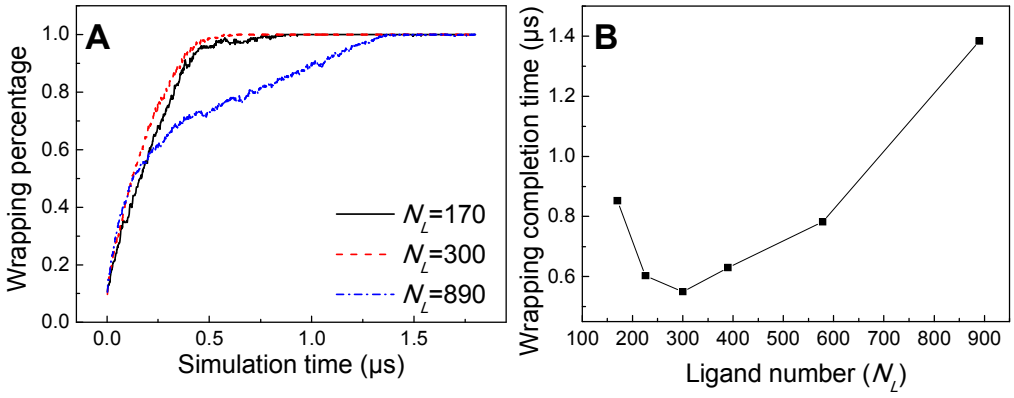

Fig. 4 Effect of ligand density on the promoting effect of cell uptake. (A) time evolution of wrapping percentage of NPs with different ligand number, (B) wrapping completion time as a function of ligand number.

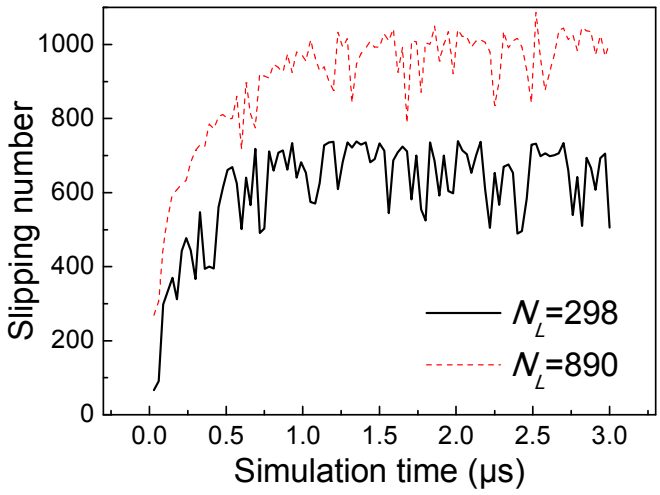

Fig. 5 Time evolutions of slipping number for NPs with different ligand density. The NP slipping number is quantified by counting the lipid molecules which were bound to ligands in the former step but free in the current step. The NP diameter and rotation speed are set to D = 15 nm and V = 0.47 degree/ns, respectively

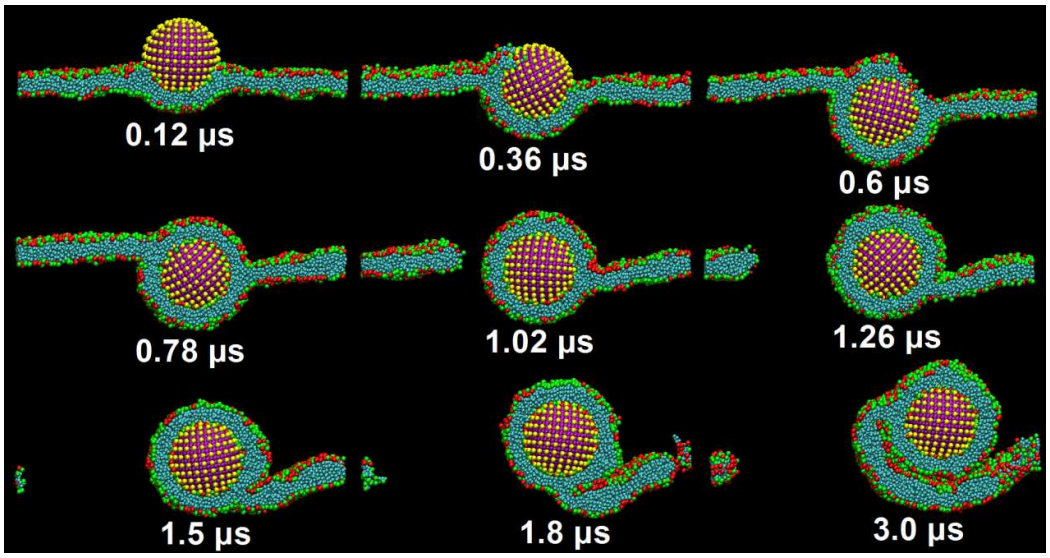

Fig. 6 Typical snapshots of promoted cell uptake (0~0.78μs) and subsequent membrane rupture (0.78~3.0μs) induced by the NP rotation. The NP size, ligand number and rotation speed are set to D = 15 nm, N_L = 261 and V = 0.57 degree/ns, respectively.

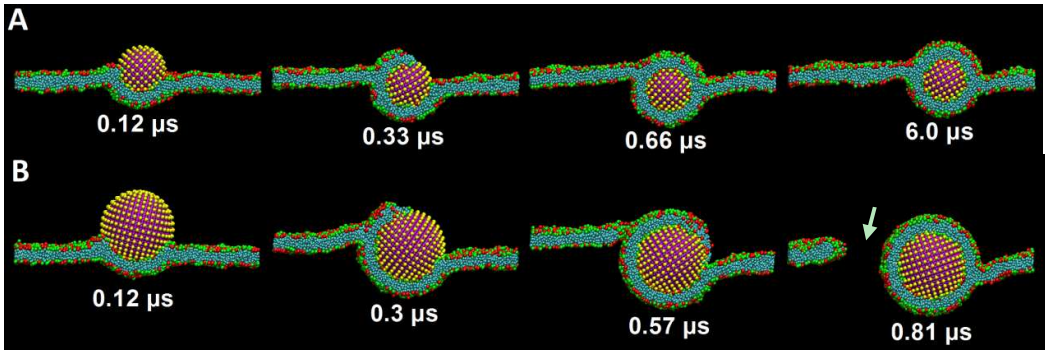

Fig. 7 Effect of NP size on the membrane response to the adsorption of rotating NPs. The NP diameter is set to D = 12.5 nm (A) and D = 20 nm (B), respectively. The rotation speed is set to V = 0.57 degree/ns. The arrow shows the membrane rupture before completion of NP wrapping.

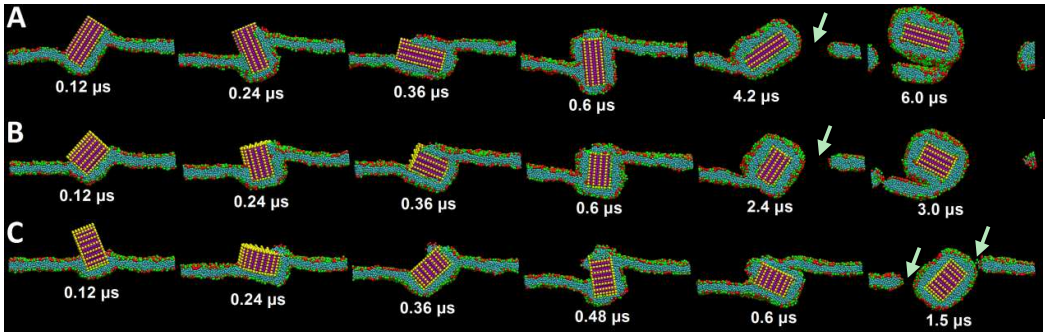

Fig. 8 Effect of NP shape anisotropy on the mechanical membrane rupture. The aspect ratio of NPs are set to L:D = 20:11 (A), L:D = 13.5:13.5 (B), and L:D = 8.0:17.4 (C), respectively. The rotation speed is set to V = 0.57 degree/ns. The arrows show the membrane rupture occasions.

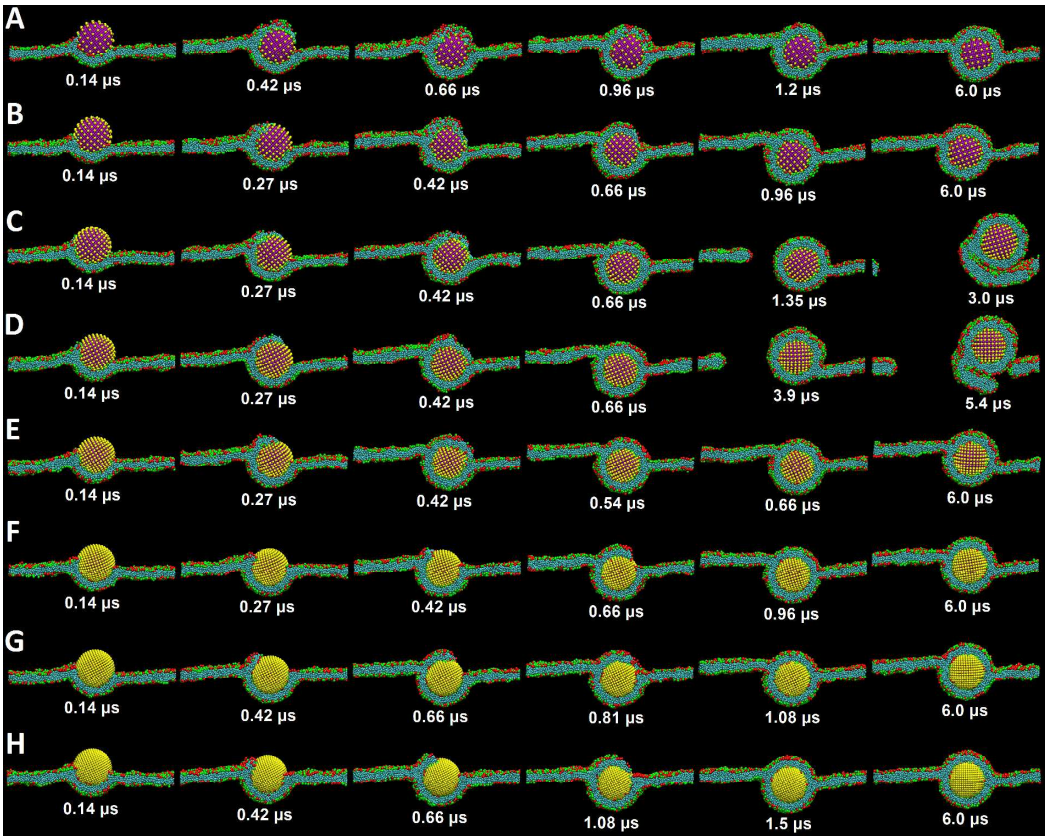

Fig. 9 Effect of ligand density on the membrane responses to the adsorption of rotating NPs. The ligand number is set to N_L = 114 (A), N_L = 170 (B), N_L = 226 (C), N_L = 298 (D), N_L = 390 (E), N_L = 578 (F), N_L = 702 (G), and N_L = 890 (H), respectively. The NP diameter and rotation speed are set to D = 15 nm, and V = 0.57 degree/ns, respectively.

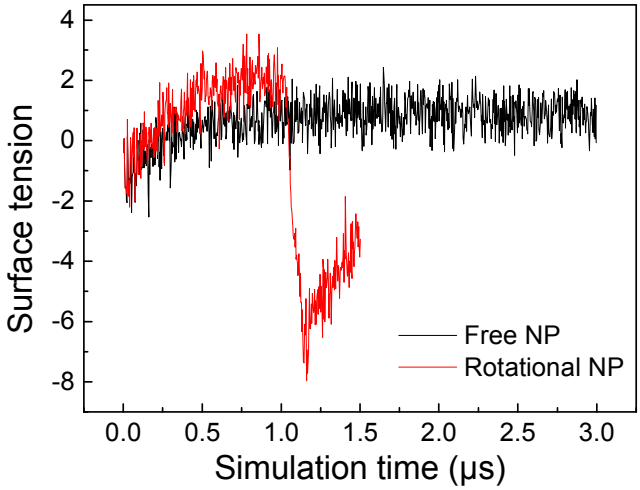

Fig. 10 Time evolutions of membrane surface tension with presence of free and rotational NPs, respectively. The sudden decrease of surface tension corresponds to the membrane rupture. The NP diameter and rotation speed are set to D = 15 nm and V = 0.57 degree/ns, respectively.

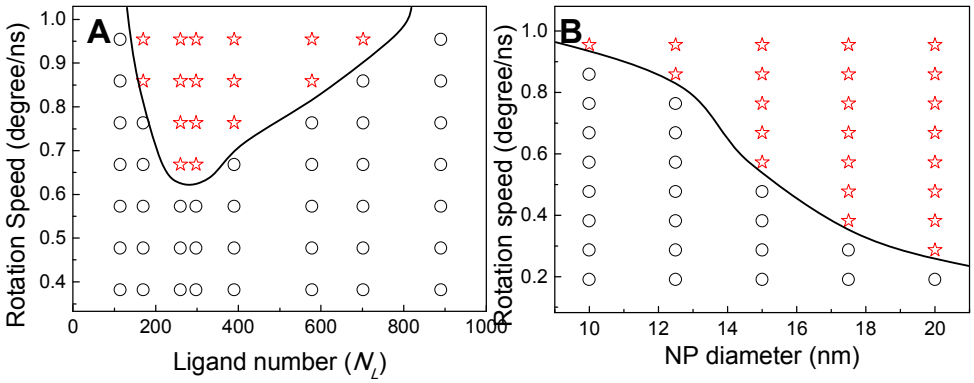

Fig. 11 Phase diagram of the membrane responses to adsorption of rotating NPs as functions of ligand density and rotation speed (A) and NP diameter and rotation speed (B). ○ represents the promoted cell uptake and ☆represents the mechanical membrane rupture.